Assessment of Luminescent Downshifting Layers for the Improvement of Light-Harvesting Efficiency in Dye-Sensitized Solar Cells

Zahra Hosseini,[a] Eric Wei-Guang Diau,[b, c] Khashayar Mehrany,[d] and Nima Taghavinia*[a, e]

Luminescence downshifting (LDS) of light can be a practical photon management technique to compensate the narrow absorption band of high-extinction-coefficient dyes in dye-sensitized solar cells (DSSCs). Herein, an optical analysis on the loss mechanisms in a reflective LDS (R-LDS)/DSSC configuration is reported. For squaraine dye (550–700 nm absorption band) and $CaAlSiN_3:Eu^{2+}$ LDS material (550–700 nm emission band), the major loss channels are found to be non-unity luminescence quantum efficiency (QE) and electrolyte absorption. By using an ideal LDS layer (QE = 100%), a less absorbing electrolyte (Co-based), and antireflection coatings, approximately 20% better light harvesting is obtained. If the absorption/emission band of dye/LDS is shifted to 800 nm, a maximal short-circuit current density (J_{sc}) of 22.1 mA cm^{-2} can be achieved. By putting the LDS layer in front of the DSSC (transmissive mode), more significant loss channels are observed, and hence a lower overall efficiency than the R-LDS configuration.

1. Introduction

All photovoltaic (PV) technologies exhibit limited spectral response to the wideband solar spectrum. This is mainly attributed to the limited absorption bands of the materials that are used as the light absorbers in solar cells.[1] In dye-sensitized solar cells (DSSCs), dye molecules are responsible for light absorption. The conventional dyes that are used in DSSCs show a reasonably wide absorption band, but on the other hand, a low absorption coefficient. This trade-off between the absorption width and absorption coefficient of dyes leads to an optimum DSSC configuration in which thick mesoporous films (> 10 μm) compensate for the low absorption coefficient of the dye. The problem is with DSSC applications in which utilization of a thick mesoporous film is not possible, for example, in solid-state DSSCs and flexible configurations.[2] In these cases, dyes with high absorption coefficient have to be used. However, the more intense light absorption comes at the expense of a narrow absorption band.[3] The high absorption coefficient of the dye can also result in lower cost of the device by providing the chance of using thin TiO₂ films.[4] To overcome the spectral losses, photon management strategies have been utilized[1a,5] among which luminescence downshifting (LDS) of the incident spectrum is a practical strategy that helps to increase the light-harvesting efficiency by manipulating the incident spectrum instead of interfering with the active material inside the cell.[1] In this approach the LDS layer, which can be used in a transmissive or reflective configuration, absorbs the high-energy photons (short wavelength) and re-emits them in lower energies (long wavelength) at which efficient dyes can absorb (shown schematically in Figure 1 and Figure 7a). In the transmissive LDS (T-LDS) structure, the incident photons pass through the LDS layer before reaching the solar cell, but in the reflective LDS (R-LDS) structure, the incident light irradiates the solar cell first.[6]

The appropriate LDS materials should possess a luminescence spectrum that matches the absorption spectrum of the solar-cell active layer. Besides, the excitation band of the LDS layer should cover well the wavelength region in which the incident photon-to-current conversion efficiency (IPCE) of the solar cell is low. To avoid the losses due to reabsorption of the emitted photons by the luminescent species in the LDS layer, the overlap between the emission spectrum and the excitation spectrum of the LDS material should be minimized. The LDS material should also have a large quantum efficiency (QE), good photostability, and low price[1] for practical applications. Suitable candidates are inorganic quantum dots (QDs), organic dyes, or inorganic phosphors. QDs exhibit a wide absorption band, high emission intensity, and relatively good photostability. However, reabsorption loss is a serious problem in using QDs due to the large overlap between their absorption and

[a] Z. Hosseini, Dr. N. Taghavinia
Institute for Nanoscience and Nanotechnology
Sharif University of Technology, Tehran 14588 (Iran)
E-mail: taghavinia@sharif.edu

[b] Prof. E. W.-G. Diau
Department of Applied Chemistry
National Chiao Tung University, Hsinchu 30010 (Taiwan)

[c] Prof. E. W.-G. Diau
Institute of Molecular Science
National Chiao Tung University, Hsinchu 30010 (Taiwan)

[d] Dr. K. Mehrany
Electrical Engineering Department
Sharif University of Technology, Tehran 14588 (Iran)

[e] Dr. N. Taghavinia
Physics Department
Sharif University of Technology, Tehran 14588 (Iran)

emission bands.[1,7] Organic dyes exhibit high absorption coefficients and high QE, but they usually have a narrow absorption band with considerable overlap with their emission band, that is, the absorption loss is a problem for organic dyes. Moreover, the photostability of organic dyes is not usually good.[1,7a] Inorganic phosphors have almost all the required characteristics for application in the LDS layer. They have good QEs, excellent photostability, and low cost. They exhibit wide absorption bands and there is usually a small or no overlap between their absorption and emission bands. Nevertheless, they have low absorption coefficient, which can be compensated by increasing the concentration of material or the thickness of the LDS layer.[1,7a,8] As a result of these characteristics, inorganic phosphors could be considered as suitable candidates for LDS applications. Herein, we study inorganic phosphors as R-LDS materials.

Since 1979 when Hovel et al. reported the first application of an LDS layer on top of PV cells,[9] several research works, both experimental and modeling, have been devoted to applying LDS layers in different kinds of solar cells.[10] These reports have mainly used the T-LDS configuration in Si solar cells,[11] CdS/CdTe solar cells,[7a,b,12] and copper indium gallium selenide (CIGS) solar cells.[13] There are a few reports on the application of LDS or luminescent downconversion materials for DSSCs. The reports were again mainly with the T-LDS configuration, and no remarkable enhancement was observed mainly due to inappropriate selection of materials or configuration.[14] Application of an LDS layer in reflective configuration for Si, CdS/CdTe, and CIGS solar cells seems not to be efficient because high-energy photons will be totally lost before reaching the LDS layer, mainly as a result of the unwanted absorption in the buffer/window layer. Nevertheless, we recently demonstrated that applying LDS materials in reflective configuration (R-LDS) may considerably enhance the light harvesting of DSSCs.[6] This was achieved by appropriate choice of a highly absorbing dye in the red/near-infrared (NIR) region (squaraine: SQ1, Figure S1 in the Supporting Information) with spectrally matching phosphors.[6] Although an increase in the efficiency of the DSSC up to 45% was already gained, clearly a comprehensive optical analysis of the LDS/DSSC device is required for understanding the optical processes involved, thereby leading to more optimum designs.

Herein, we present an optical modeling of the R-LDS/DSSC structure based on the experimental data reported previously.[6] The model can successfully reproduce the experimental external QE data. Detailed optical loss analysis of the R-LDS/DSSC stack is presented to find the configurations with the lowest loss/highest efficiency. The model provides insight on how to achieve ideal conditions with more broadband selection of dye/phosphors. In the final part, we compare the R-LDS/DSSC configuration with the T-LDS/DSSC configuration for two devices with an identical LDS layer.

2. Results and Discussion

2.1. Optical Modeling and Experimental Validation

To calculate the optical response of the system a model is employed, by which we try to reproduce the IPCE of already fabricated and characterized DSSC/R-LDS systems, as shown schematically in Figure S2. The fabrication of DSSC devices and IPCE measurements were reported elsewhere.[6] An R-LDS layer was placed in front or at the back of the cell and covered with an Al foil to reflect back the emitted light towards the DSSC.

Figure 1 illustrates the concept of an R-LDS layer coupled with a DSSC. For the red–NIR part of the light (in which SQ1
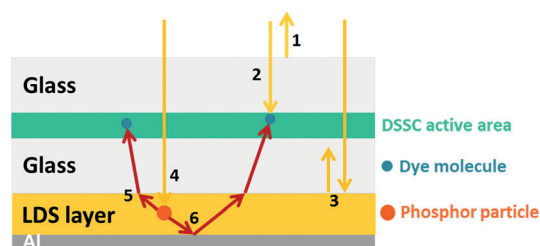

Figure 1. Schematic of the optical processes involved in the R-LDS/DSSC configuration. A fraction of incident photons will be reflected at the air/DSSC interface (1). Another fraction with wavelength in the absorption band of the sensitizing dye will be absorbed by dye molecules (2). The transmitted light from the DSSC will be either reflected back at the DSSC/LDS layer interface (3) or absorbed by phosphor particles inside the LDS layer (4). The phosphor particles then re-emit the absorbed photons at lower energies. The emitted photons will go back to the DSSC again to be absorbed by dye molecules either directly (5) or after reflection from the LDS layer/Al interface (6).

shows strong absorption), the light is absorbed either in the first passage of incident light through the DSSC or through the back-reflected light from the LDS layer. The blue–green part of the light is slightly absorbed by the dye, and is mainly downshifted by the LDS layer to red–NIR light, which returns back to the DSSC and is absorbed by the dye. Some part of the blue and green light is lost through diffuse reflection from the LDS layer or through nonradiative processes in the LDS layer.

As the incoming photons (air mass 1.5 global (AM 1.5 G) solar radiation) cross the DSSC before reaching the R-LDS layer in this reflective configuration, the total IPCE contains the original IPCE of the DSSC (without R-LDS layer) plus the improvements made by the R-LDS layer. The contribution of the R-LDS layer is either through back-reflection from the R-LDS layer or downshifting to low-energy photons. Therefore the IPCE of the DSSC with an R-LDS layer can be simply calculated as [Eq. (1)]:

$$IPCE_{R\text{-}LDS/DSSC} = IPCE_{DSSC} + IPCE_R + IPCE_{Em} \qquad (1)$$

in which $IPCE_{DSSC}$ is the IPCE of the bare device and $IPCE_R$ and $IPCE_{Em}$ are the additional contributions generated by the reflected and emitted photons from the R-LDS layer, respectively. In an ideal device with $IPCE_{DSSC} = 100\%$, no transmitted photon

from the DSSC and thereby no reflected or emitted photon from the LDS layer will exist to make a contribution to current generation. This will ensure that Equation (1) will never have a quantity greater than unity.

The distribution of reflected photons from the LDS layer ($S_R(\lambda)$) can be calculated by using the initial solar spectrum ($S_i(\lambda)$), diffuse transmission spectrum of the DSSC ($DT_{DSSC}(\lambda)$), and diffuse reflection spectrum of the LDS layer ($DR_{LDS}(\lambda)$) [Eq. (2)]:

$$S_R(\lambda) = S_i(\lambda) \cdot DT_{DSSC}(\lambda) \cdot DR_{LDS}(\lambda) \qquad (2)$$

Therefore, the IPCE$_R$ can be calculated as follows [Eq. (3)]:

$$IPCE_R(\lambda) = DT_{DSSC}(\lambda) \cdot DR_{LDS}(\lambda) \cdot IPCE_{DSSC/b}(\lambda) \qquad (3)$$

in which IPCE$_{DSSC/b}$ is the IPCE of the bare DSSC device measured counter to the illumination direction of the measurement of IPCE$_{DSSC}$ used in Equation (1). As the reflected photon flux from the R-LDS layer illuminates the DSSC from the opposite side of the initial incident photons, IPCE$_{DSSC/b}$ needs to be used in the calculation of IPCE$_R$.

In the R-LDS/DSSC configuration, there is no requirement of transparency for the LDS layer. Therefore, the thickness of the R-LDS layer can be sufficiently high to fully absorb the incident photons, which are all photons incident on the LDS layer and not reflected by this layer. With this explanation, the distribution of absorbed photons by the LDS layer ($S_A(\lambda)$) can be calculated as [Eq. (4)]:

$$S_A(\lambda) = S_i(\lambda) \cdot DT_{DSSC}(\lambda) \cdot (1 - DR_{LDS}(\lambda)) \qquad (4)$$

The number and distribution of emitted photons by the LDS layer will be defined by the QE and photoluminescence spectrum (PL(λ)) of this layer, respectively. Moreover, it is possible to put a mirrorlike layer such as an Al foil at the back of the R-LDS layer, which reflects back the emitted light in the R-LDS layer. Therefore, theoretically all the emitted photons inside the R-LDS layer can reach the DSSC either directly or after reflection from the Al foil. As the R-LDS layer is a diffuse transmitter of light (due to the granular morphology), the side-plane escape loss can be ignored. Thus, the IPCE$_{Em}$ can be calculated as [Eq. (5)]:

$$IPCE_{Em}(\lambda) = DT_{DSSC}(\lambda) \cdot (1 - DR_{LDS}(\lambda)) \cdot QE \cdot \int PL(\lambda') IPCE_{DSSC/b}(\lambda') d\lambda' \qquad (5)$$

QE is the internal quantum efficiency of the R-LDS luminescent layer and is defined as the ratio of the number of photons emitted to the number of excitation photons absorbed. Photons of wavelength λ are absorbed in the R-LDS layer and then emitted at wavelength λ' with PL(λ') spectrum. The PL spectrum should have a good overlap with the IPCE of the DSSC so that the downshifted photons can be readily converted into current. The PL(λ') used in the above equation is the normal-

ized PL spectrum of the luminescent material used in the R-LDS layer. Here, IPCE$_{DSSC/b}$ is used because of the opposite illumination direction of the emitted photon flux from the R-LDS layer relative to the initial incident photons.

The input for the optical model is the experimental data obtained by characterization of individual DSSC elements, as well as the LDS layer, presented in Figures S3 and S4. IPCE$_{DSSC}$ and IPCE$_{DSSC/b}$ are the experimental IPCE of the DSSC without R-LDS layer for different illumination directions. The transmittance of the DSSC without an LDS layer (DT_{DSSC}) can be either measured directly by using an integrating-sphere setup for the DSSC stack or calculated by using the experimental transmission measurement of all DSSC components. DR_{LDS} and PL spectra are also the experimental spectra measured by using an integrating sphere.

The optical model described above is used to calculate the IPCE of a DSSC sensitized with SQ1 dye, on which the effect of three different R-LDS layers with two illumination directions was investigated. The simulation results are compared with the experimental data reported in Ref. [6]. The R-LDS1, R-LDS2, and R-LDS3 layers were made of CaAlSiN$_3$:Eu^{2+}, Ca$_2$Si$_5$N$_8$:Eu^{2+}, and CaZnOS:Eu^{2+} inorganic phosphors, respectively. The absorption spectrum of the sensitizer (SQ1 dye) and the corresponding excitation/emission spectra of the three types of LDS films are shown in Figure S4.

Figure 2 shows the results of the calculated IPCE spectra for the three types of R-LDS/DSSC devices based on the optical model, together with the experimental data[6] under illumina-
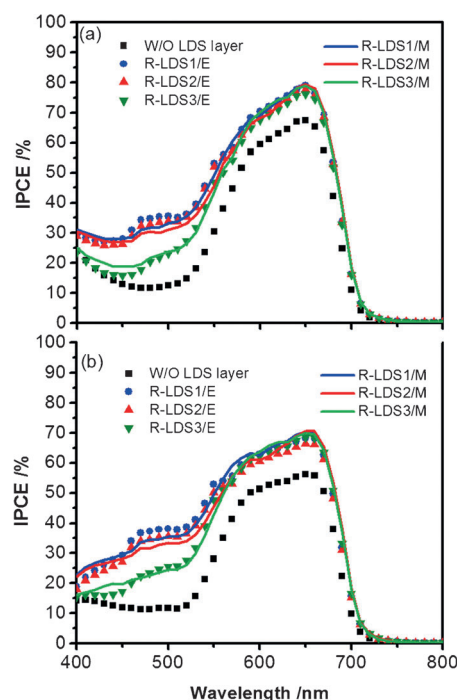

Figure 2. Calculated and experimental IPCE[6] spectra for a DSSC sensitized with SQ1 without (W/O) and with R-LDS layers for illumination from a) the WE side and b) the CE side. The symbols represent the experimental data whereas solid lines show the data based on the optical model. The R-LDS1, R-LDS2, and R-LDS3 layers are made of CaAlSiN$_3$:Eu^{2+}, Ca$_2$Si$_5$N$_8$:Eu^{2+}, and CaZnOS:Eu^{2+} inorganic phosphors, respectively.

tions from the working electrode (WE) side and counter electrode (CE) side. One observes that the model can well reproduce the experimental data. For all the R-LDS devices, the enhancement of IPCE is both in the short-wavelength region (400–550 nm) and long-wavelength region (550–800 nm), as a result of downshifting and scattering effects of the R-LDS layer, respectively. A complete discussion and comparison of the contribution of these two effects is provided in our previous report.[6] The downshifting effect is the dominant effect and the related enhancement is dependent on the R-LDS materials. The highest performance was achieved on the R-LDS1 devices under both WE side and CE side illumination, which led to relative enhancements of 40 and 54% in short-circuit current density (J_{sc}), respectively. The reason for the different results is related to the QE of the R-LDS layers and other spectral matching factors,[7a] which are discussed completely in the Supporting Information. QE seems to have a more significant contribution to the performance of the three R-LDS layers used in this research, since it is the only factor that differs considerably in these three materials (Figure S5). Because of the superior performance of the R-LDS1 layer relative to R-LDS2 and R-LDS3 layers, the following analyses presented herein are performed only on the R-LDS1 layer.

2.2. Optical Loss Analysis of the R-LDS/DSSC Device

The QE loss in an R-LDS/DSSC system can be of electrical or optical origin. In high-quality DSSCs the injection and collection efficiencies are close to unity, so one can ignore their electrical losses. However, there are several optical loss channels in this system, which are caused by the components of the DSSC devices and the R-LDS layers. Understanding these loss channels helps find solutions to improve the PV performance of an LDS-modified DSSC. The model introduced in the previous section is employed here to discriminate between the different optical loss channels.

Figure 3 displays the analysis for the R-LDS1/DSSC stack. The reflection and transmission losses along with the absorption share of each layer are calculated. By using the experimental transmission/absorption spectra of each layer of the R-LDS/DSSC stack, the absorption share of each layer on the incident photons ($S_i(\lambda)$), reflected photons from the R-LDS layer ($S_R(\lambda)$),
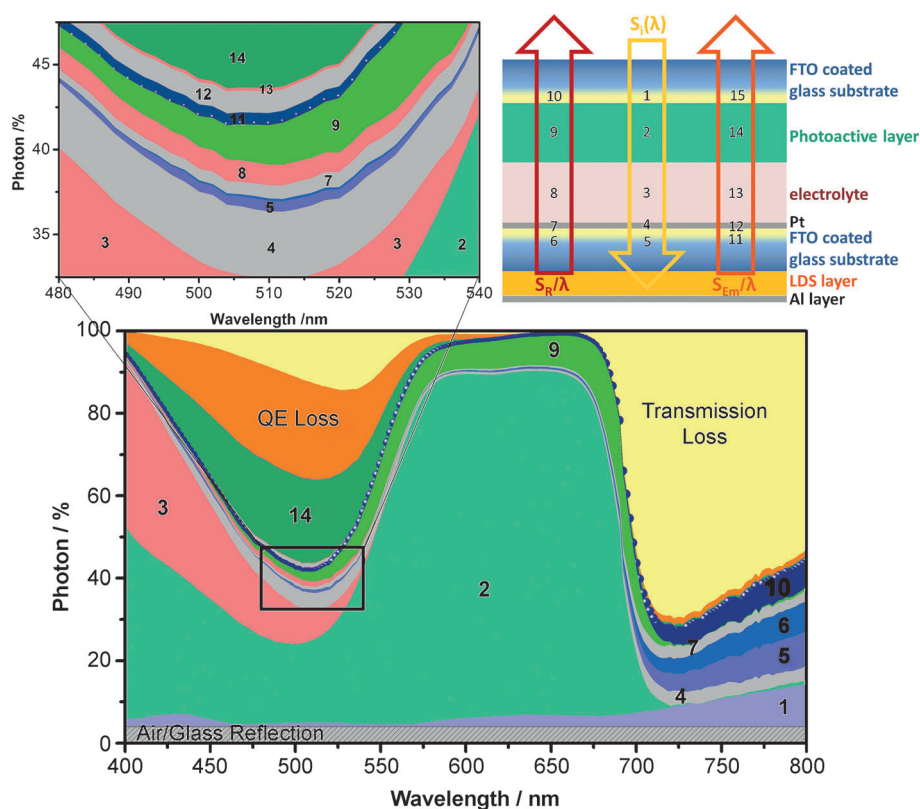

Figure 3. Optical loss analysis of the R-LDS1/DSSC device for the WE side illumination direction. FTO=fluorine-doped tin oxide.

and emitted photons from the R-LDS layer ($S_{Em}(\lambda)$) is calculated separately and illustrated in different colors. The schematic part in Figure 3 helps relate each absorption share on the graph to the corresponding material. The distribution of reflected ($S_R(\lambda)$) and emitted photons ($S_{Em}(\lambda)$) from the LDS layer can be calculated according to Equation (2) and Equation (6), respectively:

$$S_{Em}(\lambda) = \left[\int S_i(\lambda') \cdot DT_{DSSC}(\lambda') \cdot (1 - DR_{LDS}(\lambda')) \cdot d\lambda' \right] \cdot QE \cdot PL(\lambda) \quad (6)$$

The reflection at the air/glass interface has been calculated using the Fresnel equation for normal incidence. The reflection from internal interfaces in the DSSC has been neglected, due to the relatively close effective refractive indices of the materials. Moreover, there is no interference between the forward and backward traveling photons due to the incoherence nature of light. Only photons absorbed by dye molecules in the photoactive layer contribute to current generation (shown in green in Figure 3), that is, all other absorption shares are considered as loss channels. It is also clear that the highest fraction of current is generated through the initially absorbed photons by the photoactive layer. In the NIR region ($\lambda > 700$ nm) the transmission loss is noticeable, as neither dye nor the LDS layer absorbs light in this region, that is, almost all photons in the 700–800 nm range are wasted in this structure.

Moreover, the absorption by electrolyte and non-unity QE loss are another two considerable loss channels. The light absorption by electrolyte is substantial in the short-wavelength region (below 500 nm) and it blocks to some extent the excitation light for the LDS layer. Non-unity QE represents the photons absorbed in the R-LDS layer, while emitting no luminescent photons back to the DSSC. In the following sections, some approaches will be suggested to minimize these losses. The result of a similar analysis for the CE side illumination direction is available in the Supporting Information (Figure S6).

Figure 4 displays the total loss contributed by the glass reflection, FTO, electrolyte, and Pt, as well as the QE and transmission loss, for both CE and WE side illumination directions.
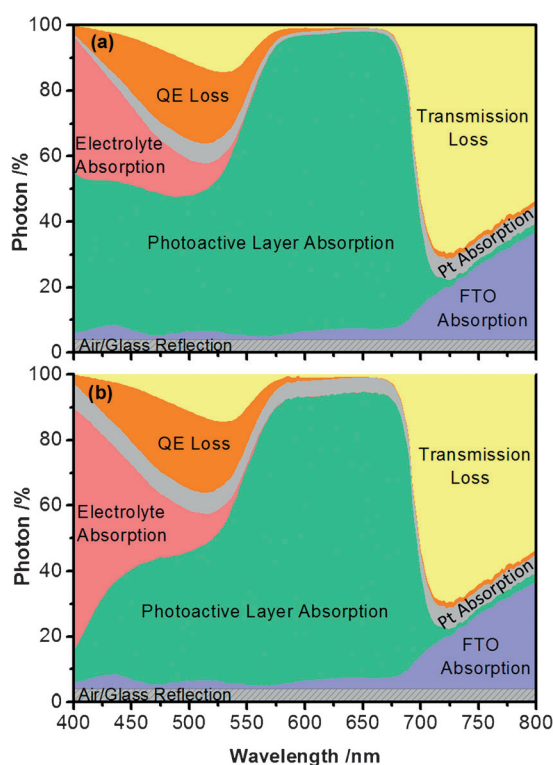

Figure 4. Total absorption by different layers of the DSSC in the R-LDS1/DSSC stack together with the reflection, transmission, and QE loss share for a) WE side illumination direction and b) CE side illumination direction.

The green part represents the light-harvesting efficiency (LHE), that is, the percent of the incident photons absorbed by the photoactive layer at each wavelength. The LHE and IPCE are related to each other by the relation: $IPCE = LHE \times \eta_{inj} \times \eta_{col}$. Here, η_{inj} is the injection efficiency of electrons from dye to the TiO_2 mesoporous body, and η_{col} is the collection efficiency of the injected electrons.

The transmission loss represents the part of light that is transmitted through the DSSC/R-LDS structure and exits out from the initial incidence direction without being absorbed. It is actually the sum of the reflected and emitted photons from the R-LDS layer, which are not absorbed by any layer of the DSSC stack. Transmission loss, as well as reflection loss, is independent of illumination direction (Figure 4). Reflection loss is

caused mainly by the air/glass interface at the first light incidence, which is the interface with highest refractive contrast.

Figure 4 also shows that the optical loss by the electrolyte is higher for CE side illumination than WE side illumination. Light absorption by the electrolyte attenuates considerably the amount of light that can be absorbed directly by the photoactive layer for the CE side illumination, and that will also lead to lower total efficiencies for this illumination direction. The extent of the electrolyte absorption, which is mainly in the 400–500 nm range, is a considerable source of loss, and can be up to 30% at 450 nm. A low fraction of loss is attributed to Pt absorption, and again for CE side illumination it is higher, as the incident light passes first through the Pt layer. The LHE of the DSSC/R-LDS (green part) is also higher for WE side illumination, which is attributed to lower loss channels in this illumination direction. The absorption losses in the FTO/glass substrates in the visible region are negligible and independent of the illumination direction.

2.3. Towards a Loss-Free R-LDS/DSSC Device

The focus of this section is to determine the potential enhancement in current density and thereby the efficiency of the R-LDS/DSSC device, which can be obtained by minimizing the optical losses. We propose some modifications to the device configuration, described in Figure 5, and calculate the attainable enhancements in ΔJ_{sc} with each modification. The ΔJ_{sc} values were calculated based on the spectral areas of LHE. In an ideal device, injection and collection efficiencies can be close to unity.[15] Therefore the IPCE of the device will be determined by the LHE. However, here we only estimate the relative changes of ΔJ_{sc} based on the spectral changes of LHE with each modification.

Figure 5a presents the LHE after application of a few practical modifications. The relative increases of J_{sc} related to each modification are also shown. Optical loss analysis of the R-LDS/DSSC device after application of all modifications for WE side illumination is shown in Figure 5b. Similar data for CE side illumination are presented in Figure S7. The first modification is application of an antireflection coating (ARC) on the DSSC to decrease the reflection at the air/glass interface. Here it is assumed that the ARC can reduce the average reflection from 4 to 1%.[16] The calculated enhancement made by the ARC is not remarkable (Figure 5a), that is, 3.1% enhancement in J_{sc}.

Another possible modification is using electrolytes with lower absorption in the blue–green region. As discussed earlier (Figures 3 and 4), the iodine-based electrolyte causes relatively high loss in the 400–500 nm range. Although we tried to use the lowest possible concentration of triiodide in the electrolyte, still 41% of the incident photons at 400 nm are absorbed by the electrolyte for WE side illumination and 74% for CE side illumination. Here it is shown that if iodine-based electrolyte is replaced with Co^{2+}/Co^{3+} electrolyte, which is more transparent,[17] the photon absorption at 400 nm will decrease to 30 and 54% for WE and CE side illumination, respectively. The total J_{sc} enhancement made by this new electrolyte (assuming no adverse effect on the electrical characteristics) is 1.5 and
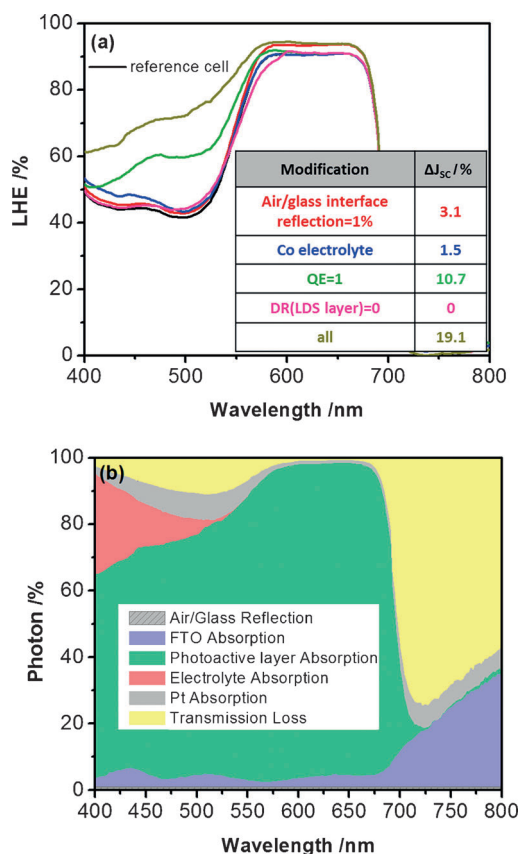
Figure 5. a) LHE (%) after application of some possible modification approaches. The contribution of each modification is presented separately, and the total effect is also shown. The value of ΔJ_{sc}% for each modification is displayed in the inset table. b) Optical loss analysis of an R-LDS/DSSC device after application of all the mentioned modifications for WE side illumination direction.

The mentioned modifications totally result in 19 and 23% J_{sc} enhancement for WE and CE side illumination, respectively. The loss analysis after these modifications, shown in Figure 5b, demonstrates a clearly improved LHE, in particular in the blue–green regions (compared to manufactured devices: Figure 4). One notes that there are still loss channels through Co electrolyte absorption, Pt absorption, and transmission loss.

The above estimations demonstrate that with the present configuration of SQ1 dye and $CaAlSiN_3:Eu^{2+}$ as the R-LDS phosphor layer, no more than about 20% efficiency enhancement is possible, compared with the experimental values that we had already reported.[6] Further improvement is possible by changing the dye/LDS match in a way to increase the absorption range of the R-LDS/DSSC device. The spectral range of the present configuration is almost below 700 nm. Therefore, we tried to select possible dye and LDS materials to increase the absorption range to 800 nm. For this purpose, VG5 dye is proposed, which is a squaraine dye with absorption band around 600–800 nm,[18] and $CaS:Yb^{2+}$ phosphor,[19] which has a good spectral match with this dye. The chemical structure of VG5 is shown in Figure S1. This selection is based only on spectral matching considerations, not efficiencies. The absorption of a TiO_2 film sensitized with VG5 dye is shown in Figure 6a along with the excitation and emission spectra of $CaS:Yb^{2+}$ in-
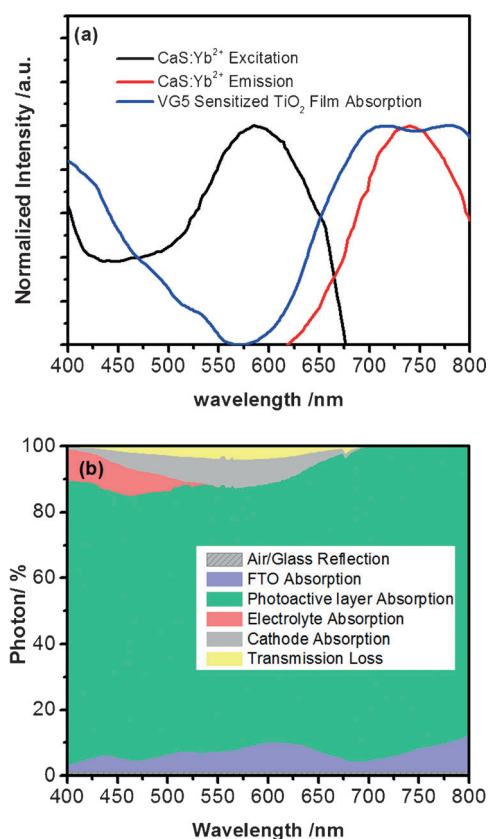
4.1% for the WE and CE side illumination directions, respectively. The enhancement is not significant, because replacement of the electrolyte only affects the spectral region below 500 nm.

Figure 5a shows that an appreciable improvement is made by modifying the QE of the LDS layer. Optimization of the synthesis process, as well as the right choice of phosphor material, results in increased QE. In ideal conditions QE is unity and all the photons absorbed by the LDS layer will be converted to low-energy photons. Here, if the QE of the R-LDS1 (51%) is assumed to be increased to 100%, then J_{sc} is improved by 11% for the WE side illumination direction. QE has the most pronounced effect on the J_{sc} improvement.

Another possible modification is through decreasing the diffuse reflectivity of the R-LDS layer. The part of light reflected from the R-LDS layer makes no contribution to the luminescence shifting signal. Changing the size of the R-LDS particles or using refractive index matching between particles and medium can be effective in reducing the diffuse reflection of R-LDS layers towards zero. Figure 5a shows that using an R-LDS layer with zero reflection will not noticeably change the J_{sc} values. The reason is that the R-LDS layer we used shows very low reflection in the absorption range of the layer, thus making little change in the overall performance.

Figure 6. a) Absorption spectrum of VG5-sensitized TiO_2 film together with the excitation and emission spectra of $CaS:Yb^{2+}$ phosphor.[18, 19a] b) Optical loss analysis of an R-LDS/DSSC device with VG5 dye as the sensitizer and $CaS:Yb^{2+}$ phosphor as downshifting material. The QE of the phosphor is assumed to be unity.

organic phosphor.[18,19] The absorption band of the phosphor covers the region in which VG5 dye does not show good absorption, and its emission band shows a good overlap with the absorption band of the dye. The optical loss analysis is performed for this R-LDS/DSSC device, similar to the previous cases. Here it is assumed that the QE of CaS:Yb^{2+} phosphor is unity. Although the spectral match of this phosphor with VG5 dye is very good, there is no reported information on the QE of CaS:Yb^{2+}, as far as we know. Nevertheless, many CaS phosphors are efficient luminescent materials and QEs of about 80% or more are routinely possible for this phosphor with many activators.[19b] Notably, not many phosphors fulfill the requirement of having an excitation band in the visible and an emission band in the NIR region.

The optical loss analysis of the R-LDS/DSSC device with the new VG5/CaS:Yb^{2+} match (assuming QE = 1) is presented in Figure 6b. The same parameters used in the calculation of Figure 5b are used here as well. The results show a remarkable improvement in the NIR region, which will lead to increased J_{sc} and thereby device efficiency. There is also an enhancement in LHE in the low-wavelength region as a result of using this new dye, which can be attributed to the high absorption by the photoactive layer in this wavelength region. This is also the reason for lower absorption loss by the electrolyte.

2.4. Comparing R-LDS/DSSC and T-LDS/DSSC Configurations

In common LDS configurations, the LDS layer is a transparent layer that is placed on top of the solar cell, that is, the T-LDS configuration. In the case of T-LDS, besides the difficulties of making a completely transparent layer in the absorption range of the solar cell, the reflection losses at the interfaces as well as the escape cone loss are fundamental challenges, which are not limiting issues in the R-LDS configuration. Here we demonstrate an optical analysis of a hypothetical T-LDS/DSSC device made from the VG5/CaS:Yb^{2+} dye/phosphor match. We consider the LDS layer as a layer with unity QE, refractive index of 2.13, and no scattering/reflection effect. The Co electrolyte is presumed to be used in the DSSC and other assumptions are the same as those used in all calculations.

Figure 7a shows the optical processes involved in a T-LDS/DSSC configuration. The incident photons will be partly absorbed in the LDS layer while the rest will transmit and enter the solar cell where they can be absorbed by the photoactive layer. The LDS layer re-emits the absorbed photons at lower energies. The emitted photons illuminate the solar cell either directly or after reflection from the LDS layer/air interface. A part of the emitted photons escapes from the front surface of the LDS layer/air interface. It is assumed that the escape loss from side planes of the LDS layer is negligible. The transmitted photons from the LDS layer can be calculated as [Eq. (7)]:

$$S_T(\lambda) = S_i(\lambda) \cdot (1-R_1) \cdot e^{-\alpha(\lambda)\cdot d} \cdot (1-R_2) \tag{7}$$

in which $S_i(\lambda)$ is the incident photon spectrum (AM 1.5 G), R_1 and R_2 are the reflection at the air/LDS interface and LDS/glass
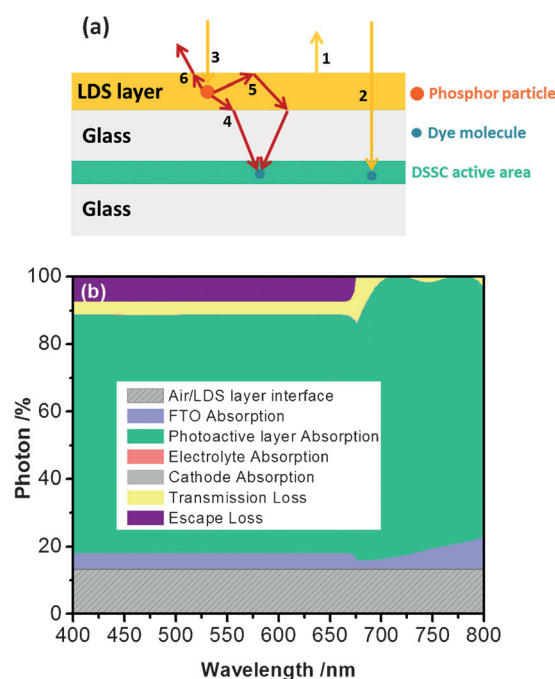

Figure 7. a) Schematic of optical processes involved in the T-LDS/DSSC configuration. A fraction of incident photons are reflected at the air/LDS layer interface (1). Another fraction with a wavelength in the absorption band of the sensitizing dye are transmitted from the LDS layer and are absorbed by dye molecules inside the DSSC (2). The high-energy photons are absorbed by phosphor particles inside the LDS layer (3). The phosphor particles then re-emit the absorbed photons at lower energies. The emitted photons go back to the DSSC to be absorbed by dye molecules either directly (4) or after reflection from the LDS layer/air interface (5). A fraction of photons emitted by the phosphor particles escape out of the LDS layer through the LDS layer/air interface (6). b) Optical loss analysis of a T-LDS/DSSC device with VG5 dye as the sensitizer and CaS:Yb^{2+} as the downshifting material. The LDS layer is considered a layer with unity QE, a refractive index of 2.13, and no scattering/reflection effect. Co-electrolyte is presumed to be used in the DSSC. The onset of LDS layer absorption is at 675 nm, which is the reason for the presence of an artifact at this wavelength.

interface, respectively, $\alpha(\lambda)$ is the absorption coefficient of the LDS layer, and d is the LDS layer thickness. The thickness of the LDS layer is supposed to be five times the penetration depth of photons at 470 nm [$d = 5(1/\alpha(470\ nm))$] to make sure all photons in the absorption range of the LDS layer can be absorbed by the luminescent material inside this layer. R_1 and R_2 are calculated from the Fresnel equations [Eqs. (8) and (9)]:

$$R_1 = \left(\frac{1-n_{LDS}}{1+n_{LDS}}\right)^2 \tag{8}$$

$$R_2 = \left(\frac{n_{LDS}-n_g}{n_{LDS}+n_g}\right)^2 \tag{9}$$

in which n_{LDS} and n_g are the refractive indices of the LDS layer and glass substrate, respectively.

The rest of the incident photons, which are not transmitted, are absorbed by the luminescent material in the LDS layer ($S_A(\lambda)$). Then the LDS layer re-emits these photons at a longer wavelength. The number of emitted photons can be determined by the luminescence QE. Having the normalized emis-

sion spectrum of the luminescent material (PL(λ)), the distribution of emitted photons ($S_{PL}(\lambda)$) can be calculated as follows [Eqs. (10) and (11)]:

$$S_A(\lambda) = S_i(\lambda) \cdot (1 - R_1) \cdot (1 - e^{-\alpha(\lambda) \cdot d}) \qquad (10)$$

$$S_{PL}(\lambda) = \left(\int S_A(\lambda') d\lambda' \right) \cdot QE \cdot PL(\lambda) \qquad (11)$$

As was discussed earlier, not all the photons emitted by the LDS layer have the chance to illuminate the solar cell. A fraction of these photons will be wasted by escaping from the front plane of the LDS layer. The final distribution of emitted photons that have the chance to illuminate the DSSC is [Eq. (12)]:

$$S_P(\lambda) = (1 - R_2) \cdot (1 - \beta(1 + R_2) \cdot S_{PL}(\lambda)) \qquad (12)$$

Here, β is the fraction of photons emitted into the angles less than the critical angle at the LDS layer/air interface [Eq. (13)]:[20]

$$\beta = \frac{1}{2} \left(1 - \sqrt{\left(1 - \left(\frac{1}{n_{LDS}} \right)^2 \right)} \right) \qquad (13)$$

The new distribution of photons by which the DSSC will be illuminated ($S_n(\lambda)$) is the sum of transmitted photons from the LDS layer ($S_T(\lambda)$) and the fraction of emitted photons that can reach the solar cell ($S_P(\lambda)$) [Eq. (14)]:

$$S_n(\lambda) = S_T(\lambda) + S_P(\lambda) \qquad (14)$$

Having the new photon flux illuminating the DSSC ($S_n(\lambda)$) together with the transmission (or absorption) spectra of different layers of the DSSC, the absorption share of each layer can be calculated. The results are shown in Figure 7b, in which the reflection, total transmission, and escape cone loss share are also presented. By comparison with the similar results for the R-LDS/DSSC (Figure 6b), two significant differences are noticeable. 1) Reflection loss is a severe problem in the T-LDS/DSSC configuration compared with the R-LDS/DSSC configuration. There is no easy way to reduce the reflection loss in this configuration, as applying ARCs on the LDS layer will increase the escape cone loss. 2) Escape cone loss exists only in the T-LDS/DSSC configuration. This means some fraction of emitted photons in the LDS layer is inevitably lost from the air interface, where the incident photons enter. In the case of R-LDS, the Al foil on the back of the R-LDS layer guarantees that all the emitted photons return to the DSSC and contribute to current generation.

Figure 8 compares the LHE (%) for the two configurations. It shows that R-LDS/DSSC is a better device configuration than the other, since there is no escape cone loss in this configuration; in addition, the application of an ARC will help to decrease the reflection loss without affecting any other optical processes. It is worth mentioning that this comparison is made for an LDS layer with no scattering, which is a necessary condi-
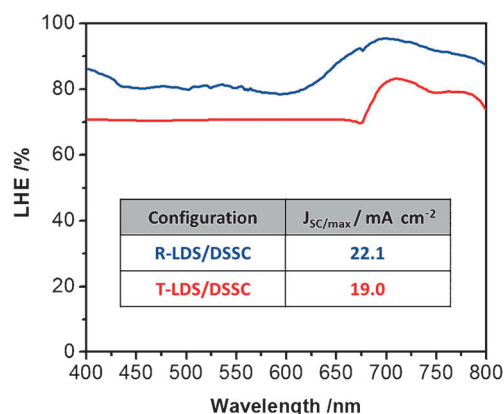

Figure 8. LHE (%) for the R-LDS/DSSC and T-LDS/DSSC configurations with identical LDS layers and DSSC devices. In the inset, the estimated total current density is reported, assuming ideal injection and collection efficiency for the DSSC device.

tion for an effective performance of the LDS layer in the T-LDS/DSSC configuration. If the LDS layer is even slightly scattering, it leads to a large loss in the T-LDS/DSSC configuration, whereas it will add functionality to the R-LDS layer and will let it operate as a scattering layer as well as downshifting layer. The maximum achievable J_{sc} values calculated with unity injection and collection efficiencies are presented in the inset table of Figure 8. VG5 is not a conventional DSSC dye and there is not sufficient information on the injection efficiency. The maximum achievable current density calculated here for the R-LDS/DSSC configuration is in good agreement with the maximum current density for a DSSC with absorption onset at 800 nm calculated by Snaith,[21] which confirms that the R-LDS idea has potential for compensating the absorption losses in DSSC devices.

3. Conclusions

We have presented a comprehensive optical model to simulate the light-harvesting performance of LDS/DSSC devices in a reflective configuration. The optical model is validated by comparing the IPCE spectra of the simulated results with those of the experimental data for three different LDS layers applied on a DSSC sensitized with SQ1 dye. Quantified figures of merit of R-LDS1, R-LDS2, and R-LDS3 layers were investigated to give the major factors responsible for the outperformance of the R-LDS1 layer relative to the other R-LDS layers. Optical loss channels were investigated for the R-LDS1/DSSC device under different illumination directions. Non-unity QE and light absorption by the electrolyte were shown to be the most significant loss channels. Applying an ARC at the air/glass interface, using Co electrolyte, optimizing the QE of the phosphor, and matching the refractive index in the LDS layer were proposed as the major modification approaches for performance improvement. Our calculations showed that the proposed optical modifications will lead to enhancements in J_{sc} by 19 and 23% for illuminations from the WE and CE sides, respectively. A broader light-harvesting feature of the device is achievable by changing the dye/phosphor match in the R-LDS/DSSC device. For

this purpose, the VG5/CaS:Yb^{2+} couple was selected as an efficient dye/phosphor system for the optical modeling performed for devices with the R-LDS and T-LDS configurations. Our simulation results indicate that the device with an R-LDS configuration attained a maximal J_{sc} value (22.1 mA cm^{-2}) that is superior to that with a T-LDS configuration (19.0 mA cm^{-2}), which is attributed to the presence of two important loss channels in the T-LDS configuration, namely, reflection loss and escape cone loss.

[1] a) X. Huang, S. Han, W. Huang, X. Liu, *Chem. Soc. Rev.* **2013**, *42*, 173–201; b) E. Klampaftis, D. Ross, K. R. McIntosh, B. S. Richards, *Sol. Energy Mater. Sol. Cells* **2009**, *93*, 1182–1194.

[2] a) U. Bach, P. Comte, J. E. Moser, F. Weisso, M. Gratzel, *Nature* **1998**, *395*, 583–585; b) H. J. Snaith, L. Schmidt-Mende, *Adv. Mater.* **2007**, *19*, 3187–3200; c) H. J. Snaith, R. Humphry-Baker, P. Chen, I. Cesar, S. M. Zakeeruddin, M. Grätzel, *Nanotechnology* **2008**, *19*, 424003; d) T. Yamaguchi, N. Tobe, D. Matsumoto, T. Nagai, H. Arakawa, *Sol. Energy Mater. Sol. Cells* **2010**, *94*, 812–816.

[3] a) A. Hagfeldt, G. Boschloo, L. Sun, L. Kloo, H. Pettersson, *Chem. Rev.* **2010**, *110*, 6595–6663; b) B. E. Hardin, E. T. Hoke, P. B. Armstrong, J. Yum, P. Comte, T. Torres, J. M. J. Frechet, K. Nazeeruddin, M. Gratzel, M. D. McGehee, *Nat. Photonics* **2009**, *3*, 406–411.

[4] S. Mathew, A. Yella, P. Gao, R. Humphry-Baker, B. F. E. Curchod, N. Ashari-Astani, I. Tavernelli, U. Rothlisberger, M. K. Nazeeruddin, M. Grätzel, *Nat. Chem.* **2014**, *6*, 242–247.

[5] a) N. Park, *Korean J. Chem. Eng.* **2010**, *27*, 375–384; b) J.-H. Yum, E. Baranoff, S. Wenger, M. K. Nazeeruddin, M. Grätzel, *Energy Environ. Sci.* **2011**, *4*, 842–857; c) S. K. Balasingam, M. Lee, M. G. Kang, Y. Jun, *Chem. Commun.* **2013**, *49*, 1471–1487.

[6] Z. Hosseini, W.-K. Huang, C.-M. Tsai, T.-M. Chen, N. Taghavinia, E. W.-G. Diau, *ACS Appl. Mater. Interfaces* **2013**, *5*, 5397–5402.

[7] a) D. Alonso-Álvarez, D. Ross, B. S. Richards, *Proc. Photovoltaic Specialists Conf.* **2012**, 9–14; b) S. D. Hodgson, W. S. M. Brooks, A. J. Clayton, G. Kartopu, V. Barrioz, S. J. C. Irvine, *Nano Energy* **2013**, *2*, 21–27; c) A. Apostoluk, Y. Zhu, B. Canut, B. Masenelli, J.-J. Delaunay, K. Znajdek, M. Sibiński, *Phys. Status Solidi* **2013**, *1307*, 1301–1307; d) S. D. Hodgson, W. S. M. Brooks, A. J. Clayton, G. Kartopu, D. A. Lamb, V. Barrioz, S. J. C. Irvine, *Prog. Photovoltaics Res. Appl.* **2013**, DOI: 10.1002/pip.2408.

[8] H. Lian, Z. Hou, M. Shang, D. Geng, Y. Zhang, J. Lin, *Energy* **2013**, *57*, 270–283.

[9] H. J. Hovel, R. T. Hodgson, J. M. Woodall, *Sol. Energy Mater.* **1979**, *2*, 19–29.

[10] a) R. Rothemund, *Sol. Energy Mater. Sol. Cells* **2014**, *120*, 616–621; b) A. M. Gabr, J. F. Wheeldon, R. M. Beal, A. Walker, J. Sacks, M. Rachel, T. J. Hall, R. N. Kleiman, K. Hinzer, *Proc. Photovoltaic Specialists Conf.* **2012**, 48–52; c) D. Alonso-Álvarez, D. Ross, E. Klampaftis, K. R. Mcintosh, S. Jia, P. Storiz, T. Stolz, B. S. Richards, *Prog. Photovoltaics Res. Appl.* **2014**, DOI: 10.1002/pip.2462.

[11] a) C. P. Thomas, A. B. Wedding, S. O. Martin, *Sol. Energy Mater. Sol. Cells* **2012**, *98*, 455–464; b) J. Liu, K. Wang, W. Zheng, W. Huang, C.-H. Li, X.-Z. You, *Prog. Photovoltaics Res. Appl.* **2013**, *21*, 668–675; c) F. Bettiol, B. S. Richards, K. R. McIntosh, G. Lau, J. N. Cotsell, K. Hanton, *Prog. Photovoltaics* **2009**, *17*, 191–197.

[12] a) D. Ross, E. Klampaftis, J. Fritsche, M. Bauer, B. S. Richards, *Sol. Energy Mater. Sol. Cells* **2012**, *103*, 11–16; b) B. S. Richards, K. R. McIntosh, *Prog. Photovoltaics* **2007**, *15*, 27–34.

[13] E. Klampaftis, D. Ross, S. Seyrling, A. N. Tiwari, B. S. Richards, *Sol. Energy Mater. Sol. Cells* **2012**, *101*, 62–67.

[14] a) J. Liu, Q. Yao, Y. Li, *Appl. Phys. Lett.* **2006**, *88*, 173119–173122; b) H. Hafez, M. Saif, M. S. A. Abdel-Mottaleb, *J. Power Sources* **2011**, *196*, 5792–5796.

[15] T. W. Hamann, R. A. Jensen, A. B. F. Martinson, H. Van Ryswyk, J. T. Hupp, *Energy Environ. Sci.* **2008**, *1*, 66–78.

[16] K. B. Blodgett, Reduction of Surface Reflection. US patent No. 2220861A, **1940**.

[17] A. Yella, H.-W. Lee, H. N. Tsao, C. Yi, A. K. Chandiran, M. K. Nazeeruddin, E. W.-G. Diau, C.-Y. Yeh, S. M. Zakeeruddin, M. Grätzel, *Science* **2011**, *334*, 629–634.

[18] C. Magistris, S. Martiniani, N. Barbero, J. Park, C. Benzi, A. Anderson, C. Law, C. Barolo, B. O'Regan, *Renewable Energy* **2013**, *60*, 672–678.

[19] a) W. Yen, M. Weber, *Inorganic Phosphors: Compositions, Preparation and Optical Properties*, CRC Press, Boca Raton, **2004**; b) W. Lehmann, *J. Lumin.* **1972**, *5*, 87–107.

[20] B. Hong, *Sol. Energy Mater. Sol. Cells* **2003**, *80*, 417–432.

[21] H. J. Snaith, *Adv. Funct. Mater.* **2010**, *20*, 13–19.